

Influence of boundary conditions on the characteristics of nuclear fissionPavel V. Kostryukov^{✉*} and Artur Dobrowolski*Theoretical Physics Department, Maria Curie-Skłodowska University, 20-031 Lublin, Poland*

(Received 3 April 2023; accepted 20 July 2023; published 15 August 2023)

In this work, we carried out a detailed study of the factors affecting the fission dynamics of selected even-even actinide nuclei within a quasiclassical statistical approach based on the Langevin formalism. Essentially, the influence of initial conditions and geometrical criteria for spontaneous and induced fission of ^{236}U as for the test case are worked out and then, using the knowledge thus acquired, we perform more extensive calculations for selected nuclei of U, Pu, Cm, Cf, and Fm isotopic chains. Potential energy surfaces (PES) are calculated within a macroscopic-microscopic approach in a three-dimensional space of the so-called Fourier deformation parameters representing the square of surface radius function in cylindrical coordinates. We also use the Lublin-Strasbourg Drop and folded-Yukawa mean-field models to estimate the full PES for these isotopes. The restoration of the particle number in the superfluid BCS-like approach is realized within the generator coordinate method with the Gaussian Overlap Approximation in the one-dimensional gauge-angle space. The tensors of inertia and friction, which play the role of transport coefficients, are given respectively within the hydrodynamic Werner-Wheeler approximation and what we usually call the “wall” formula. The main part of our research focuses on studying the conditions imposed on the solutions of the Langevin equations. In particular, we analyze the effect of the initial point distribution used to generate Langevin trajectories on resulting fragment mass and total kinetic energy distributions. Furthermore, we derive a way to optimize the size of the neck showing up on a nuclear surface in the final stage of its evolution to fission, taking into account the random and sudden natures of its rupture. Neck thicknesses generated with an appropriate normal distribution reproduce reasonably well the empirical fragment mass distributions in the lighter actinides along various excitation energies. However, for heavier actinides, such as Cf and Fm, the capability of our model to reproduce the final fragmentation seems to be limited.

DOI: [10.1103/PhysRevC.108.024605](https://doi.org/10.1103/PhysRevC.108.024605)**I. INTRODUCTION**

This year marks the 85th anniversary of the discovery that heavy atomic nuclei are not only radioactive but can also, under certain conditions, decay into fragments with variable mass numbers, which was called the fission process. Although fission has been intensively studied over this long time, we still do not have complete knowledge of the process. Of course, in the second half of the previous century, many successful attempts were made to describe it theoretically, which led to the development of various known macroscopic-microscopic models based on a description of the energy of a fissioning nucleus analogous to that of a deformed liquid droplet with additional corrections for interactions of a quantum nature, realized most often by the Strutinsky approach and the Bardeen-Cooper-Schrieffer (BCS) model of superfluidity, respectively (see, e.g., Refs. [1–8]), providing a correct description of fission characteristics, such as fragment mass distributions (FMD), fragment charge distributions (FCD), total kinetic energy (TKE) distributions, a multiplicity of emitted particles, etc. One of the above-mentioned research directions is coupling the macroscopic-microscopic approach with the multidimensional stochastic Langevin equations,

which can describe the evolution of nuclear fission as a stochastic process. As computational power increases, this method is continuously improved, for example, by adding additional degrees of freedom on which the resulting fragment mass (charge) or total kinetic energy distributions may depend. Currently, there are several operative models using this method [9–20]. For instance, the models acting in three-dimensional (3D) collective spaces are presented in Refs. [10,11,15,17,18,20] while the four-dimensional (4D) spaces are exploited, e.g., in Refs. [12,13,16,19]. Nevertheless, there are still uncertainties in the description of the dynamics of the phenomenon under study, especially at its final stage, when the fissile system is close to decaying into fragments.

The starting point of our research is the construction of a potential energy function based on the well-known nuclear theory Strutinsky-type macroscopic-microscopic approach [2,3], where the function in question depends on collective degrees of freedom, here taken as deformation parameters of the nuclear surface. The nuclear surface geometry is defined by the shape parametrization, which is given here as a Fourier expansion of the square of the distance of a given point on the surface to the symmetry axis, $\rho^2(z, \varphi)$. The amplitudes of such a linear combination standing in front of the sine and cosine functions are related to the deformation parameters of the potential energy surface (PES) [21]. The fission dynamics,

*kostr@kft.umcs.lublin.pl

where the evolution of the surface shape is governed by the system of Langevin equations [22], is described by a set of classical Hamilton-like trajectories, taking into account the excitation energy, friction between moving nucleons, and diffusion effects. Particular attention is paid to investigating and testing the initial and the trajectory-termination conditions, which are crucial in obtaining a reasonable agreement of the generated mass distributions of primary fission fragments with the empirical data. The presented model has been “calibrated” to characterize in the best possible way the dynamics induced by thermal and 15 MeV neutron fission of the ^{235}U nucleus. Afterward, with further minor generalizations, it was applied to simulate the spontaneous and induced fission of compound even-even actinides with proton numbers Z in the region 92–100.

The work has the following structure: After a general introduction, the second section is devoted to the main points of the model. In the third section, we investigate the dependence of evaluated distributions of the primary fission fragments on the initial and termination conditions for the Langevin trajectories. In the fourth section, we apply the model developed above to other than ^{236}U even-even actinide nuclei and discuss the quality of our results, comparing them with existing empirical data. In the final section, we summarize our results.

II. QUASICLASSICAL STOCHASTIC LANGEVIN APPROACH

The precise determination of the deformation parameters $\{q_i\}$ relevant to the fission process and the tensors of collective inertia and friction are necessary for successfully applying the Langevin formalism to simulate the evolution of the nucleus toward fission. The key issue of this kind of quasistochastic model is to obtain a realistic change of the shape of the nuclear surface over time, which will be achieved by accumulating a large number of Langevin trajectories $\mathbf{q}(\mathbf{t}) = \{q_1(t), \dots, q_N(t)\}$ in the assumed N -dimensional space of collective variables.

At present, there exist various nuclear shape parametrizations, among which the most popular are spherical-harmonic decomposition [23], Cassini ovaloids [24,25], Funny-Hills and its later variations [4,26], or two-center shell model (TCSM) parametrization [27]. Nevertheless, this article uses a relatively new, efficient, and fast convergent parametrization [21], which represents the axially symmetric nuclear surface in cylindrical coordinates, $\rho_s^2(z; \mathbf{a})$, as a Fourier expansion of the form

$$\rho_s^2(z; \mathbf{a}) = R_0^2 \sum_{n=1} \left[a_{2n} \cos \left(\frac{2n-1}{2} \pi \frac{z-z_{sh}}{z_0} \right) + a_{2n+1} \sin \left(\frac{2n}{2} \pi \frac{z-z_{sh}}{z_0} \right) \right], \quad (1)$$

where $R_0 = 1.2A^{1/3}$ is the radius of the corresponding spherical nucleus, and z_{sh} is the displacement of the center of mass of the deformed nucleus when $a_{2n+1} \neq 0$ is considered. It would be useful to define the auxiliary dimensionless parameter $c(\mathbf{a})$ responsible for elongating the nuclear body along the z axis. If $c > 1$, nuclear shapes are *prolate*, whereas $c < 1$ produces

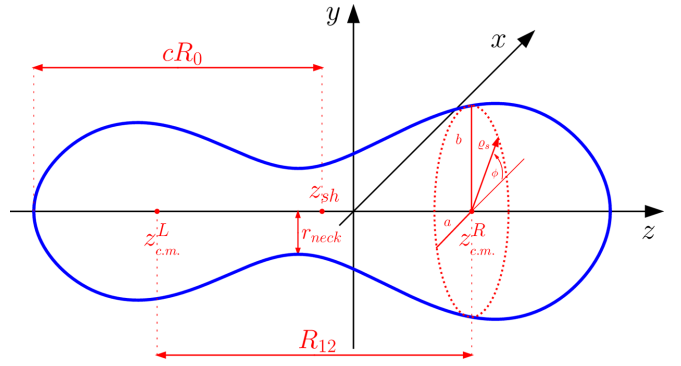


FIG. 1. An example of the elongated nuclear surface obtained in the Fourier parametrization (1).

oblate shapes. Therefore, the length of the nucleus measured along the z axis is $2z_0 = 2cR_0$, where $\pm z_0$ determines the position of the right and the left ends of the nucleus in case $z_{sh} = 0$. In expansion (1), the coefficients a_n are not yet the physical deformation parameters. It was proved, e.g., in Ref. [21] that the transformation between original $\{a_n\}$ amplitudes in the Fourier series (1) and the physical deformation parameters $\{q_n\}$ can be of the following form:

$$\begin{aligned} q_2 &= a_2^0/a_2 - a_2/a_2^0, \\ q_3 &= a_3, \\ q_4 &= a_4 + \sqrt{(q_2/9)^2 + (a_4^0)^2}, \\ q_5 &= a_5 - (q_2 - 2)a_3/10, \\ q_6 &= a_6 - \sqrt{(q_2/100)^2 + (a_6^0)^2}. \end{aligned} \quad (2)$$

The parameters a_2^0, a_4^0, a_6^0 describe, via Eq. (1), the spherical shape with radius R_0 .

To discuss the influence of nonaxial surface shapes, one can easily modify our shape parametrization by multiplying the right-hand side of Eq. (1) by a function $f_\eta(\varphi)$ of the nonaxiality parameter η defined as

$$f_\eta(\varphi) = \frac{1 - \eta^2}{1 + \eta^2 + 2\eta \cos \varphi}, \quad (3)$$

chosen in such a way that any cross section of the nuclear drop (1), perpendicular to the z axis, is an ellipse of half axes a and b while $\eta \equiv \frac{b-a}{b+a}$. The geometric properties of a nonaxial, prolate nuclear surface are presented schematically in Fig. 1, whereas a series of shapes possible to obtain through Eq. (1) configurations is visualized in Fig. 2.

It was investigated that the most relevant deformation parameters for fission process, $\{q_2, q_3, q_4\}$, describe the nuclear elongation along the z axis, mass (volume) asymmetry of the left and right fragments, and the neck shape, respectively. It should be noted that the results presented in Refs. [21,28] reveal that the set of these three collective deformations, $\mathbf{q} = \{q_2, q_3, q_4\}$, is sufficient to describe the behavior of the fissioning system close to its scission point within a reasonable energetic uncertainty of much less than 1 MeV. Therefore, the

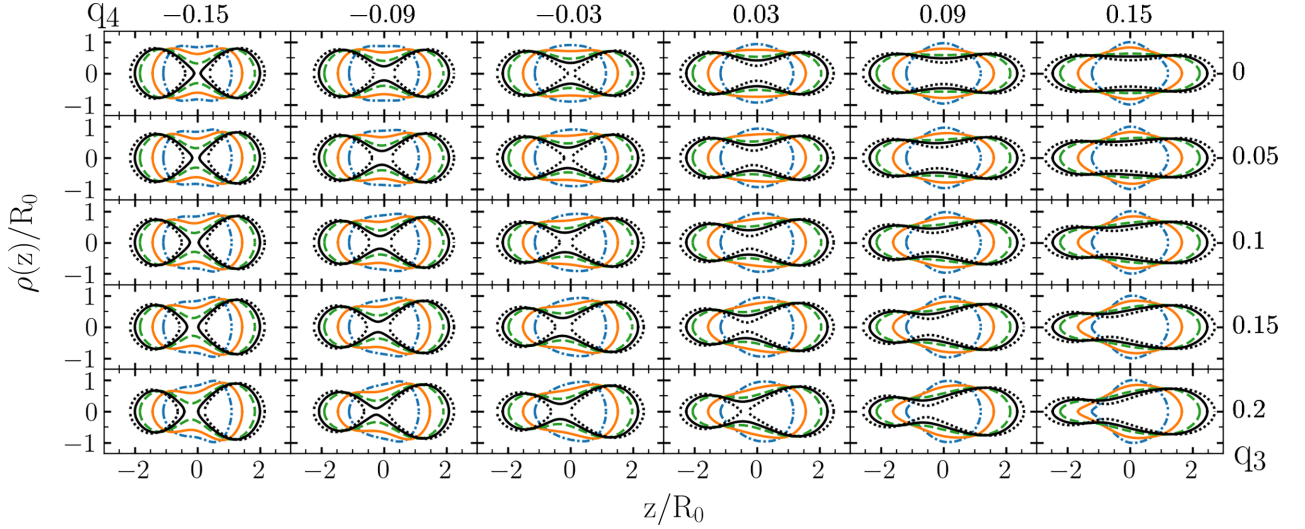


FIG. 2. Fourier-like surface shapes for $q_2 = 0.3$ (blue dot-dashed line), $q_2 = 1$ (green dashed line), $q_2 = 1.9$ (orange solid line), $q_2 = 2.35$ (black solid line), and $q_2 = 2.9$ (black dotted line).

higher-order deformations, q_5 and q_6 , which mainly modify the shapes of fission fragments in an insignificant way, are neglected at the current stage of our study.

A similar argumentation may be applied to the nonaxiality degree of freedom, which is known to impact the PES of, in particular, actinide nuclei in the region between the ground state and the inner fission barrier by reducing its height within 0.5–1 MeV. Thus the above property of the PES allows us, to a first approximation, to neglect the effect of the nonaxial deformation η as being of minor importance for nuclear fragmentation.

A. Potential energy surface

Setting the geometry of the nuclear surface, we come to the problem of defining the potential energy function, which is an essential quantity determining the evolution of the fissile system. As already mentioned, from among a wide range of known approaches able to produce the potential energy function depending on the surface shape, we decided to use a well-known macroscopic-microscopic model. Then, the total energy of a nucleus, $V(\mathbf{q})$, can be composed of the leading macroscopic term E_{macr} , evaluated using a liquid-drop-type approach, while the microscopic interaction energy E_{micr} , playing the role of the energy correction on top of the dominating smooth liquid-drop term, is strictly related to the specific single-particle structure of a given nucleus,

$$V = E_{\text{macr}} + E_{\text{micr}}. \quad (4)$$

The deformation-dependent smooth energy contribution E_{macr} in Eq. (4) is given through the macroscopic Lublin-Strasbourg drop (LSD) energy term [29]

$$\begin{aligned} E_{\text{LSD}} = & b_{\text{vol}}(1 - k_{\text{vol}}I^2)A \\ & - b_{\text{surf}}(1 - k_{\text{surf}}I^2)A^{2/3}B_{\text{surf}}(\mathbf{q}) \\ & - b_{\text{cur}}(1 - k_{\text{cur}}I^2)A^{1/3}B_{\text{cur}}(\mathbf{q}) \end{aligned}$$

$$\begin{aligned} & - \frac{3}{5}e^2 \frac{Z^2}{r_0^{\text{ch}}A^{1/3}}B_{\text{Coul}}(\mathbf{q}) + C_4 \frac{Z^2}{A} \\ & - 10 \exp(-4.2|I|), \end{aligned} \quad (5)$$

where $I = \frac{N-Z}{A}$ is the so-called reduced isospin, whereas B_{surf} , B_{cur} , and B_{Coul} functions introduce the deformation dependence on the surface, curvature, and Coulomb energy contributions, respectively. The last deformation-independent term is what we usually call the congruence energy and is taken from the estimates of Myers and Swiatecki [1]. All parameters of the LSD formula originally found in Ref. [29] are also rewritten below:

$$\begin{aligned} b_{\text{vol}} &= 15.4920 \text{ MeV}, & k_{\text{vol}} &= 1.8601, \\ b_{\text{surf}} &= 16.9707 \text{ MeV}, & k_{\text{surf}} &= 2.2038, \\ b_{\text{cur}} &= 3.8602 \text{ MeV}, & k_{\text{cur}} &= -2.3764, \\ C_4 &= 0.9181 \text{ MeV}, & r_0^{\text{ch}} &= 1.21725 \text{ fm}. \end{aligned}$$

Please notice that this simple formula has been proven to reproduce the ground-state masses of over 3000 isotopes and over 80 fission barriers throughout the periodic table with reasonable accuracy.

In turn, the microscopic part, E_{micr} , in Eq. (4) is customarily decomposed into two energy components responsible for the shell, E_{shell} , and pairing interaction (superfluidity), E_{pair} , effects simulated within the BCS model, proposed in Ref. [30]. The shell correction E_{shell} is, by definition, obtained by subtracting the mean energy \tilde{E} arisen due to smoothing out the nucleon mean-field spectrum up to the levels belonging to the energy continuum from the sum of all the occupied single-particle energies e_k (see, e.g., Ref. [31]) as

$$E_{\text{shell}} = \sum_k e_k - \tilde{E}. \quad (6)$$

In Eq. (6), the averaged energy \tilde{E} is estimated through the Strutinsky method [2,3] by smearing out the discrete spectrum with the Hermite “correction” polynomial of sixth order.

Finally, the pairing energy correction is determined in a similar way as done in Eq. (6), but the resulting BCS energy is, in addition, reduced by the so-called average pairing-energy term \tilde{E}_{pair} , which is not accounted for in the smooth liquid-drop contribution (5), as done in Ref. [32]:

$$E_{\text{pair}} = E_{\text{BCS}} - \sum_k e_k - \tilde{E}_{\text{pair}}. \quad (7)$$

The single-particle spectra for protons and neutrons of the actinide nuclei discussed here are obtained as the eigenvalues of the folded-Yukawa mean-field Hamiltonian as described in Ref. [31].

B. Nuclear shape evolution

As mentioned, to describe the fission dynamics of selected actinide nuclei, we use a quasiclassical stochastic model, widely presented in Ref. [22], where a compound, excited, and in a general rotating nucleus, is represented in the form of an evolving-in-time superfluid incompressible drop [4] with a well-defined deformed surface. Its time evolution is governed by the set of coupled Langevin equations as a function of collective deformation variables $\{q_i(t)\}$ and the corresponding canonically coupled momenta $\{p_i(t)\}$:

$$\begin{aligned} \frac{dq_i}{dt} &= \sum_j [\mathcal{M}^{-1}]_{ij} p_j, \\ \frac{dp_i}{dt} &= - \left[\frac{1}{2} \sum_{jk} \frac{\partial [\mathcal{M}^{-1}]_{jk}}{\partial q_i} p_j p_k + \frac{\partial F}{\partial q_i} \right. \\ &\quad \left. + \sum_{jk} \gamma_{ij} [\mathcal{M}^{-1}]_{jk} p_k \right] + \mathcal{R}_i, \end{aligned} \quad (8)$$

where \mathcal{M}_{ij} and γ_{ij} are tensors corresponding to mass (inertia) and intrinsic friction, respectively, while F is the Helmholtz free energy potential of the compound fissile system,

$$F(\mathbf{q}, T) = V(\mathbf{q}) - a(\mathbf{q})T^2. \quad (9)$$

In the above, $a(\mathbf{q})$ is, in general, the deformation-dependent energy level density obtained according to the prescription in Ref. [33] and T is the temperature of the system, which is related to the excitation energy E^* through the relation

$$E^* = a(\mathbf{q})T^2. \quad (10)$$

It is assumed in our work that the excitation energy, E_0^* , at the initial time $t = 0$ is given relative to the ground state and the height of the fission barrier, V_B .

The last term, \mathcal{R}_i , in the second of Eqs. (8), corresponds to the i -th component of the Langevin random force, which by definition is

$$\mathcal{R}_i = \sum_j g_{ij} \Xi_j(t), \quad (11)$$

where $\Xi(t)$ is a time-dependent stochastic function given as $\Xi_j(t) = \xi_j/\sqrt{t}$ with the following properties: $\langle \xi_k \rangle = 0$, $\langle \xi_k \xi_l \rangle^2 =$

2. The amplitudes g_{ij} can be deduced from the fluctuation-dissipation theorem [22,34], known as the Einstein relation allowing calculation of the diffusion tensor

$$\mathcal{D}_{ij} \equiv \sum_k g_{ik} g_{jk} = \gamma_{ij} \cdot T, \quad (12)$$

with γ_{ij} denoting the friction tensor. The collective inertia used in Eqs. (8) is calculated within the incompressible irrotational flow approach using the Werner-Wheeler approximation [35],

$$\mathcal{M}_{ij}(\mathbf{q}) = \pi \rho_m \int_{z_{\min}}^{z_{\max}} dz \rho_s^2(z, q) \left[A_i A_j + \frac{1}{8} \rho_s^2(z, q) A_i' A_j' \right], \quad (13)$$

where $\rho_m = M_0 / (\frac{4}{3} R_0^3)$ is the average uniform nuclear density with $M_0 = 0.0113 A^{5/3}$, the coefficients A_i having the form

$$A_i = \frac{1}{\rho_s^2(z, \mathbf{q})} \frac{\partial}{\partial q_i} \int_z^{z_{\max}} \rho_s^2(z', \mathbf{q}) dz'. \quad (14)$$

Since our discussion is limited to low-energy fission, using the one-body approach to describe the γ_{ij} friction tensor is convenient. Then such a dissipation friction-tensor component may be expressed through the so-called wall formula [36] as

$$\gamma_{ij}^{\text{wall}} = \frac{\rho_m}{2} \bar{v} \int_{z_{\min}}^{z_{\max}} \frac{\frac{\partial \rho_s^2}{\partial q_i} \frac{\partial \rho_s^2}{\partial q_j}}{\sqrt{4\rho_s^2 + \left(\frac{\partial \rho_s^2}{\partial z}\right)^2}} dz. \quad (15)$$

In the above, \bar{v} is the average intrinsic velocity of nucleons, the value of which can be evaluated within the Fermi gas model to be $\bar{v} = \frac{3}{4} v_F$ with v_F being nucleon velocity at the Fermi level.

C. Temperature effects

As it follows from Eq. (9), the system of Langevin equations (8) has an additional hidden parameter, namely, the temperature T , which is necessary to obtain a correct solution in the case of substantially excited systems. The information about the change of T during nuclear shape evolution from the initial to final prescission state can be extracted from the conservation of the total energy, which must be constant at each time along a given trajectory and is composed of the kinetic and potential terms and the excitation energy of intrinsic degrees of freedom E^* :

$$E_{\text{total}} = \frac{1}{2} \sum_{jk} [\mathcal{M}^{-1}]_{jk} p_j p_k + V(\mathbf{q}, T) + E^*. \quad (16)$$

It is well known that the microscopic component of the total potential energy (4) vanishes when the temperature increases. To account for this effect, the dependence of the exponential form $e^{-E^*/\text{const}}$ to modify the shell correction was proposed by Ignatyuk *et al.* in Ref. [37]. A few years later, a similar dependence appeared also for pairing correction [38]. One of the most recent works on this topic is Ref. [39], where the reduction of both the shell and pairing microscopic corrections with excitation energy for deformed nuclei are revisited.

In our model, however, we use a slightly modified prescription of this temperature correction in the form of a Fermi-type

function, discussed in Refs. [28,33]:

$$E_{mic}(\mathbf{q}, T) = \frac{E_{mic}(\mathbf{q}, T = 0)}{1 + e^{-\frac{T_E - T}{a_E}}}, \quad (17)$$

with $T_E = 1.5$ MeV and $a_E = 0.3$ MeV. It was proved in Refs. [17,28] that such a relationship could reliably describe the evolution of the FMDs with increasing excitation energy.

Hence, as the excitation energy grows, the viscosity of the nuclear liquid must increase, too, and finally, its superfluid properties must drastically fade away. As shown in Ref. [40], the temperature dependence of the friction tensor must have a similar form as the above shell correction and is written

$$\gamma_{ij}^T(\mathbf{q}, T) = \frac{0.7}{1 + e^{-\frac{T_\gamma - T}{a_\gamma}}} \gamma_{ij}^{\text{wall}}(\mathbf{q}, T = 0) \quad (18)$$

with the constants $T_\gamma = 0.7$ MeV and $a_\gamma = 0.25$ MeV providing a good description of the dissipative properties of the diffusion tensor D_{ij} of Eq. (12). The introduced temperature dependence significantly changes the friction when T tends to zero, which happens, e.g., in spontaneous fission. As known, classical Brownian motion vanishes when the system's temperature tends to zero. Thus the diffusion tensor D_{ij} , which fixes the magnitude of the random Langevin force, should vanish, too, and therefore, the statistical nature of the fission processes will be violated. On the other hand, quantum-mechanical considerations bring us to an obvious conclusion that even with temperature being close to zero, i.e., for very low excitation energy, the zero-point motion of nucleons can cause fission.

To simulate these quantum effects in the semiclassical Langevin description, one can replace the temperature T with an effective temperature T^* in Eq. (12), as proposed in Ref. [41]:

$$T^* = E_0 \coth \frac{E_0}{T}, \quad (19)$$

where $E_0 = \frac{\hbar\omega_0}{2}$ roughly corresponds to a nucleus's zero-point collective oscillation energy near its ground state, which typically varies between 0.5 and 2 MeV. Under this assumption, one obtains from Eq. (12) a more realistic description of the intrinsic friction in low-energy fission.

With all the above approximations, we can now solve the set of Langevin equations (8) using the discretization method in which the corresponding differential quotients are applied instead of the time derivatives occurring on the left-hand sides of both equations. The finite time step for the numerical solution of their discretized forms is taken as 0.01τ , where $\tau \equiv \frac{2\mathcal{M}}{\gamma} \frac{\hbar}{\text{MeV}}$ is called the characteristic relaxation time, sufficient to ensure the thermal equilibrium of the nuclear system.

III. INITIAL AND TRAJECTORY-TERMINATING CONDITIONS

Having described the essential components of the model, we can proceed toward one of the key points of this work, namely, defining the set of boundary conditions for the differential Langevin equations. For this purpose, first, one should define a region in the domain of collective variables \mathbf{q} in which

the shape evolution of a nucleus is to be performed. Some detailed studies have shown that for the majority of actinide nuclei, it is sufficient to consider the following collective three-dimensional deformation space,

$$\begin{aligned} q_2 &= [0 (0.05) 2.35], \\ q_3 &= [-0.21 (0.03) 0.21], \\ q_4 &= [-0.21 (0.03) 0.21], \end{aligned} \quad (20)$$

which comprises vicinities of the ground state, all relevant for fission-process saddle points and isomeric minima ending within the configurations, where the nucleus is already split into two fragments. The latter statement may mean that the width of the neck of a compound nucleus is sufficiently small compared with the effective diameter of a nucleon ($\approx 0.2R_0$) to observe the fission. In the nodes of such a lattice, we have calculated the previously introduced values of the collective potential, inertia, and friction tensors. To determine the values between the nodes, we use the so-called Gauss-Hermite approximation method proposed in Ref. [42], which determines the demanded values on, generally, N -dimensional mesh with pretty satisfactory accuracy.

Let us mention the behavior of a trajectory when a variable q_i , being a part of the parametric definition of that, reaches its extreme (border) value given in Eqs. (20). This may happen, for example, when the entry point in a given isotope is located relatively close to the grid boundaries and, therefore, after a couple of time steps, can easily reach the border. Technically, such a trajectory does not lead to fission and, strictly speaking, should be removed from our consideration. In such a case, some conditions for resuming such a trajectory may be helpful. A reasonable possibility to omit this problem may be to change the sign of the momentum component conjugated to this coordinate, allowing it to turn around and continue its evolution.

The situation is slightly exceptional with the *leading* coordinate q_2 . After reaching its extreme value $q_2^{\text{max}} = 2.35$ [see relation (20)], the system is elongated more than twice that in its ground state. Suppose that for such a large deformation, the decisive criterion for qualifying a given trajectory as the fissioning one is still not fulfilled. In that case, such a trajectory seems to have no physical sense, and its further evolution is meaningless. Hence, this basic condition must be imposed in most further calculations, mainly if a symmetric and highly elongated fission channel is intensely populated.

A. Adjusting the initial conditions

We initiate the evolution of a Langevin trajectory by choosing its initial deformation point on the PES. In general, such a point is assumed to be the ground state of the compound system, as it is done in the classical works of Abe [22,43]. In order to be able to describe its evolution into different decay channels, the compound system must initially remain close to its ground state. However, in practical calculations, a thus-defined starting configuration usually needs to be adjusted to a given particular nucleus and its excitation energy to effectively determine a set of thousands of stochastic trajectories within

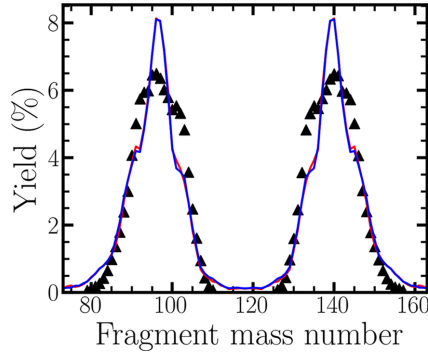


FIG. 3. Primary FMDs for thermal neutron-induced fission of ^{235}U initiated from the ground state (red) and the second saddle (blue), whereas black triangles correspond to values adapted from experimental data [45]. Here $Y(A_f)$ denotes the yield for the corresponding fragment mass.

a reasonable time scale. In fission, the available energy excess has, at least, to be enough for the system to overcome the barriers standing in the way of the fissioning nucleus. Thus, the set of initial configurations drawn at the beginning of each trajectory is likely located in a specific area in the vicinity of the outer saddle point, through which the system must pass, moving towards fission.

To test the above assumption, we first calculate the fragment mass distributions for the thermal neutron-induced fission of a ^{235}U nucleus starting from two different initial configurations. The first and most natural option is to initiate the trajectory from the ground state. Afterward, to compare the results, the trajectories begin in the outer saddle point. In both cases, the initial conjugated momenta are all equal to zero.

As a nucleus is assumed to undergo fission, the determination of the corresponding trajectory is terminated if the neck radius in the thinnest point reaches $r_{\text{neck}}^{\text{stop}} \approx (0.2-0.3)R_0 \approx 1.5$ fm on average (for comparison, see, e.g., Res. [10,18,44]). To some extent, such a criterion is chosen arbitrarily. It can be modified by introducing a dependence of r_{neck} on the precision deformation (elongation) or temperature in the scission point. Technically, as the temperature increases, the neck collapses faster, with larger neck thicknesses. Clues supporting this hypothesis will be given later. As seen in Fig. 3, the fragment mass distributions for both these cases are almost identical. The total number of trajectories used here to generate reliable statistics is significant and equal to 10^5 . Only 1 out of 100 initiated in the ground-state trajectories overcome the barrier and efficiently evolve to fission. At the same time, the rest are stuck in the potential energy well for a long time. If, however, calculations begin in the immediate vicinity of the outer saddle point, the number of “trapped” trajectories is lower by practically an order of magnitude.

By introducing a method proposed in Refs. [17,46], one can still improve the ratio of “passed” to “trapped” trajectories. Using the normal distribution $\xi_{\text{norm}}(\mu, \sigma)$ with the mean value $\mu = 0$ and the standard deviation of $\frac{1}{2}\sqrt{\frac{E_0}{\partial^2 V}}_{\partial q_i^2}$ defined in the prefixed starting point $\mathbf{q}^{\text{start}}$, we define the set of initial

spatial configurations $\mathbf{q}^{(1)}$ of subsequent trajectories through the following condition:

$$q_2^{(1)} \geq q_2^{\text{start}},$$

$$V(\mathbf{q}^{\text{start}}) - V(\mathbf{q}^{(1)}) - E_0 \equiv E_{\text{kin}}^{(1)} \geq 0, \quad (21)$$

where $E_{\text{kin}}^{(1)}$ is the kinetic energy of collective motion in the initial point of a given trajectory calculated through the classical relation as

$$E_{\text{kin}}^{(1)}(\mathbf{q}^{(1)}) = \frac{1}{2} \sum_{ij} [\mathcal{M}^{-1}(\mathbf{q}^{(1)})]^{ij} p_i^{(1)} p_j^{(1)}. \quad (22)$$

The constant E_0 in the second condition of Eqs. (21) describes a contribution of the zero-point vibrations to the total potential energy in $\mathbf{q}^{\text{start}}$. The values of momenta $p_k^{(1)}$, like the coordinates $\mathbf{q}^{(1)}$, must be randomly distributed. The mean (standard) deviation for the i th momentum component within its normal distribution ξ_{norm} is $\sigma = E_{\text{kin}}^{(1)} \mathcal{M}_{ii}(\mathbf{q}^{(1)})$. To finally identify the randomly chosen momenta p'_i with actual components of $p_i^{(1)}$ entering the Langevin equations as their initial value, they need to be renormalized as

$$p_k^{(1)} = p'_k \sqrt{\frac{E_{\text{kin}}^{(1)}}{\frac{1}{2} \sum_{ij} [\mathcal{M}^{-1}]_{ij} p'_i p'_j}}$$

to satisfy condition (21).

The question arises whether the space of $\mathbf{q}^{(1)}$ points should be restricted to a specific volume around the $\mathbf{q}^{\text{start}}$ point. In terms of condition (21), such a problem may occur when the PES is sufficiently flat around this point, allowing the initial configuration to exceed the borders of the fixed grid [see Figs. 4(a) and 4(c)]. To avoid this, we can limit the deformation space $\mathbf{q}^{(1)}$ of the initial configurations by a slightly arbitrary interval as follows:

$$q_2^{(1)} \in [q_2^{\text{start}}; q_2^{\text{start}} + 0.2],$$

$$q_3^{(1)} \in [q_3^{\text{start}} - 0.09; q_3^{\text{start}} + 0.09],$$

$$q_4^{(1)} \in [q_4^{\text{start}} - 0.09; q_4^{\text{start}} + 0.09]. \quad (23)$$

In Fig. 4, we can see the PES for ^{236}U , where the coordinates $\mathbf{q}^{(1)}$ are distributed without [Figs. 4(a) and 4(b)] and with [Figs. 4(c) and 4(d)] the zero-point energy in Eq. (21) or with and without limitations for the initial coordinate region [Figs. 4(b) and 4(d)]. In particular, the two curves of Figs. 5(c) and 5(d) reveal the lack of sensitivity of the FMD for these limitations. In this case, the ratio of traversed to not traversed trajectories in Fig. 5(d) falls within the interval 1–1.5, noticeably reducing the computation time.

B. Fissioning trajectories

Having determined the criteria for fixing the starting point for a Langevin trajectory, let us now turn to the problem of the rupture of the fissile system. In reality, the division of a nucleus into fragments may significantly depend not on the neck width alone but also on a series of other quantities characterizing bulk and surface properties of both fragments, their shell structures, deformations, excitation energies, the

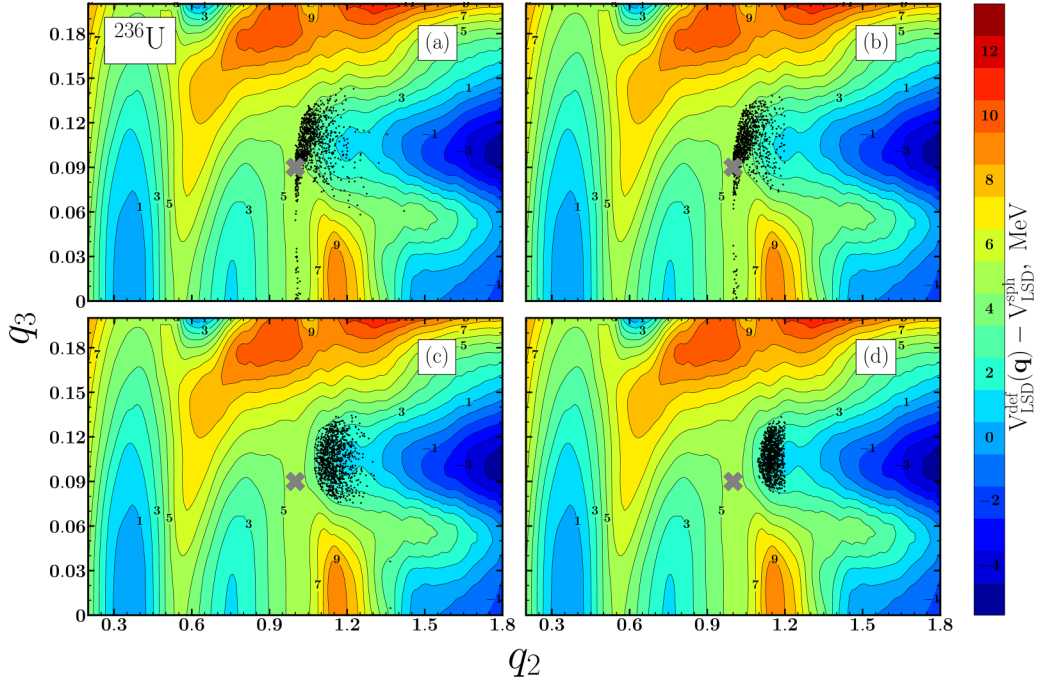


FIG. 4. Samples of starting-point distributions on the PES of ^{236}U : (a) without limit control, and subtraction of E_0 , (b) without limit control, and inclusion of E_0 , (c) without control, and inclusion of E_0 , and (d) with limit control, and E_0 included. The gray cross gives the location of the second saddle.

relative collective velocity of fragments towards fission, neck curvature, etc. Knowing the decisive criteria for stopping the trajectory evolution due to the achievement of a neck-breaking configuration is even more crucial than choosing its starting point. Unfortunately, this problem is not unambiguously solvable at the moment. It requires the introduction of additional phenomenological assumptions, which will only be tested by comparing the simulation results with empirical data. That, in turn, can definitively reduce the transparency and universality of this approach.

Since the phenomenological criteria for the neck rupture are model dependent and can be fixed to some extent arbitrarily, we decided to test within this work the one which effectively would lead to a division of an axial nucleus into

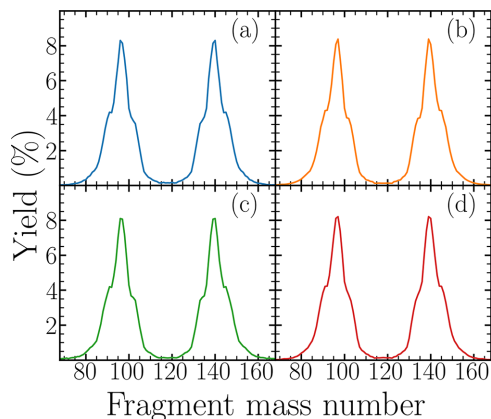


FIG. 5. Primary FMDs obtained for starting-point distributions presented in Fig. 4. Panels (a)–(d) refer to analogous panels of Fig. 4.

two fragments and depending only on the neck radius value, r_{neck} . By collecting the configurations which satisfy the required condition, e.g., $r_{\text{neck}}^{\text{stop}} = \text{const}$, we obtain the precision hypersurface in the multidimensional space of deformation variables. It was tested in our approach that a nucleus has a chance to split into two fragments when the neck radius varies in the range 0–2.5 fm with a mean value of about 1 fm, being comparable to the effective radius r_n of a single nucleon residing inside the neck. Similar termination conditions in terms of nonzero neck width are considered in Refs. [9,10,15,18,44].

There also exists another point of view on the neck size criterion, in which splitting into fragments occurs when $r_{\text{neck}} = 0$; i.e., the thickness of the neck at the thinnest point vanishes. Indeed, this approach makes it possible to precisely determine the masses and kinetic energies (TKE) of the fragments of such a binuclear shape because their volumes and relative distances are determined unambiguously. This kind of condition was exploited in Refs. [11–13,16,19], where the mean field was given in the form of the two-center Nilsson-like potential allowing for a reasonably credible description of the single-particle spectra at the neck rupture deformation. In contrast, within a similar model, good results can also be achieved if one fixes $r_{\text{neck}}^{\text{stop}} = 0.5$ fm (see, e.g., Ref. [15]). One can observe in Fig. 2 that already all shapes at the upper limit $q_2^{\text{max}} = 2.35$ and the values of $q_4 < \approx -0.15$ are split into two fragments, whereas for higher q_4 s they are still single shaped. Therefore, theoretically, not all trajectories passing through the limit of q_2^{max} must result in fission. Obviously, the number of fission acts may depend here on the particular choice of $r_{\text{neck}}^{\text{stop}}$. In practice, the topography of the PES and the inertia parameters in the ^{236}U nucleus at $q_2 > 2.35$ indicate that the number of actually obtained trajectories with $r_{\text{neck}}^{\text{stop}} > 0$ may

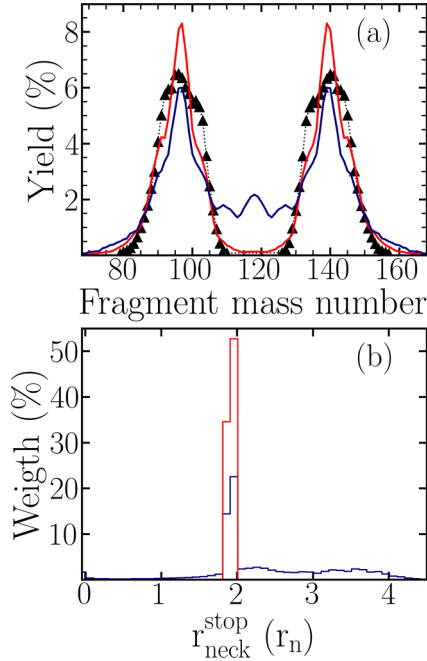


FIG. 6. Primary FMDs (a) for thermal neutron-induced fission of ^{235}U with obligatory usage of neck radius condition (red) and without it (navy blue). (b) The histogram shows the r_{neck} distribution for both (a) and (b) cases.

occur for thermal neutron-induced fission, relatively small and feeding mostly moderately asymmetric yields.

Since the present calculations are carried out on a finite deformation grid, the grid-border values are usually fixed slightly before the *geometrical scission*, i.e., where the neck radius is strictly equal to zero. This is so because the uncertainty of numerical determination of the PES and necessary transport quantities for the two strongly elongated fragments already well separated by the zero-width neck are considerably lowered due to limitations of numerical routines used to develop the eigensolutions of the Yukawa-folded Hamiltonian and the liquid-drop deformation functions.

However, in specific test cases shown below, where the pre-scission configurations for symmetric fission can be strongly elongated, we allow for the possibility that the trajectory is continued even though the above-mentioned elongation limit, q_2^{max} , is slightly exceeded. At the same time, the condition for the neck radius is still not satisfied.

To depict the contribution of such strongly elongated states to the final FMD, in addition to the previously developed initial conditions (23), we will introduce the trajectory-termination conditions in two ways. First, for elongations, $q_2 < q_2^{\text{max}}$, a trajectory that satisfies only the neck-radius criterion, $r_{\text{neck}} < r_{\text{neck}}^{\text{stop}}$, is counted as a fissioning one. In the case $q_2 > q_2^{\text{max}}$ and when the neck radius is still greater than a fixed $r_{\text{neck}}^{\text{stop}}$ value, such a trajectory is then rejected. This scenario is shown in Fig. 6(a) with the red line. In contrast, we consider the second way, where the neck radius condition is completely ignored, and the trajectory reaching the elongation limit q_2^{max} describes the act of fission unequivocally. Clearly, in the latter

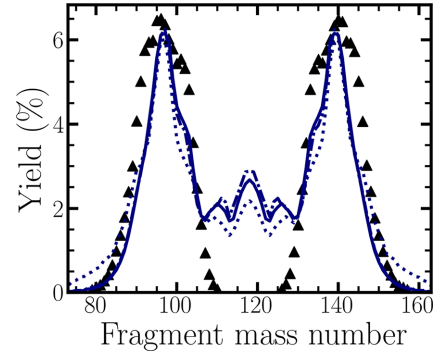


FIG. 7. Primary FMDs for thermal neutron-induced fission of ^{235}U with nonobligatory neck radius condition usage at limit values $q_2^{\text{max}} = 2.35$ (dotted line), $q_2^{\text{max}} = 2.5$ (dash-dotted line), and $q_2^{\text{max}} = 2.9$ (solid line).

scenario, the values of the neck radii in the fissile configurations distribute over different possible values ranging from r_n to even more than $4r_n$ with a clear peak around $2r_n$, as presented in Fig. 6(b) with the navy blue line.

As shown in Fig. 6(a), neglecting the condition $r_{\text{neck}}^{\text{stop}} > r_{\text{neck}}$ leads to significant enhancement of both near-symmetric and highly asymmetric channels compared to the experimental yields. To clarify this, let us return to Fig. 2, where, among other things, the shapes with $q_2 = q_2^{\text{max}} > 2.35$ are tested for neck radius value. Indeed, it can be seen that at such a limit of q_2^{max} , only compact-shaped and rather mass-asymmetric configurations prefer the neck radius around $(0-0.3)R_0$, which favors fissioning in low excitation energy regimes. In contrast, very elongated fragmentation modes are relatively less populated. The increase of mostly asymmetric FMD fission yields with a gradual shift of q_2^{max} from 2.35 to 2.9 visible in Fig. 7 can therefore be found as a consequence of an undesirable property of our Fourier shape parametrization which, especially for extremely large nuclear elongations q_2 , is unable to produce well-separated ($r_{\text{neck}} \approx 0$) very elongated symmetric fragments which may appear in the fission of thorium and uranium isotopes. This disadvantage is essentially removed in an upgraded version of the Fourier-like parametrization, which is currently being extensively tested.

One then deduces that the conditions for nuclear scission applied to our Langevin framework, which mainly determines the quality of reproduction of FMD, have to be sought according to the following indications: first, by considering pure geometrical criteria for the neck width, dependent only on the surface-parametrization properties, and second, by testing, whereas, for such a preselected deformation point, the accuracy of determining the macroscopic-microscopic quantities fits the acceptable limits. This also indicates that the choice of the optimal $r_{\text{neck}}^{\text{stop}}$ value may not, in general, be universal across the complete set of studied nuclei and needs, at least, to be validated when changing Z or N by a couple of units.

C. Optimal neck radius

Now, after demonstrating that the condition for the neck size is essential, let us investigate its effect on the distributions

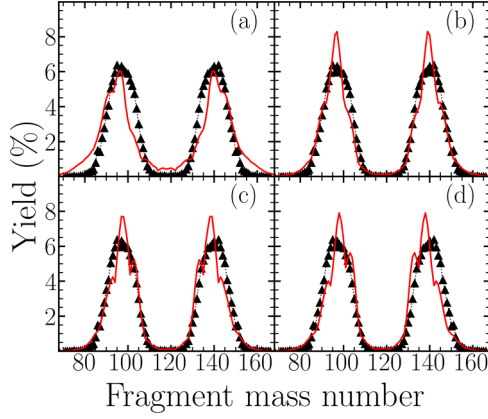


FIG. 8. Primary FMDs for neutron-induced fission ^{235}U with variation of the neck radius r_{neck} from (a) $3r_n$, (b) $2r_n$, (c) r_n , and (d) 0.

of the fission mass fragments. For this purpose, we assume that the corresponding value of the neck radius $r_{\text{neck}}^{\text{stop}}$ limit at which a trajectory is stopped may vary from $3r_n$ to as low as zero with a step of r_n . We set the initial point according to the prescription of Eq. (23) while the upper elongation limit $q_2^{\text{max}} = 2.35$. As can be seen from Fig. 8, the resulting mass distributions noticeably change their form for different $r_{\text{neck}}^{\text{stop}}$ radii. With decreasing neck radius, the fragment mass distribution is getting slightly narrower, and the asymmetric peak shifts towards more and more symmetric yields. At the same time, its symmetric part is gradually vanishing, approaching the experimental value.

To understand the dominance of the asymmetric fission channel in this nucleus, let us notice at the PES presented in Fig. 4 that the most likely path from the starting configuration, set around the second saddle point at $(q_2, q_3) \approx (1.0, 0.09)$, to the scission leads directly towards the asymmetric valley which is separated from the symmetric one by the edge almost 3 MeV high, visible around $q_3 \approx 0.06$. Moreover, since the excitation energy at the initial configuration is relatively low, the random force defined through Eqs. (11) and (12) has little chance to push the system over this edge. It can also be seen

that except for the extreme cases of Figs. 8(a) and 8(d) with $r_{\text{neck}}^{\text{stop}} = 3r_n$ and $r_{\text{neck}}^{\text{stop}} = 0$, respectively, the overall features of other presented distributions are generally weakly affected, which may indicate that the main contributions to the final FMD come from $r_{\text{neck}}^{\text{stop}} = \{2r_n, r_n, 0\}$.

D. Stochastic character of neck breaking

Taking into account the results shown in Fig. 8, one can ask whether the use of the strictly fixed value of $r_{\text{neck}}^{\text{stop}}$ which governs the moment of splitting of a nucleus into fragments of different masses (charges) is not a severe simplification of the stochasticity of the fission phenomenon. A simplistic realization of the idea of, to some extent, a random value of the $r_{\text{neck}}^{\text{stop}}$ radius just before the neck breaking is to draw at the beginning of each trajectory its value from a specific interval, say, $[0, \alpha_r r_n]$, with a probability given through the uniform distribution. The fragment mass distributions shown in Fig. 9 are calculated for the following three values: $\alpha_r = \{1, 2, 3\}$. The results are compared with the FMD obtained within analogous intervals as in Figs. 8(a)–8(c), respectively.

The above concept may also be realized if instead of the uniform discrete distribution of $r_{\text{neck}}^{\text{stop}}$ one uses the continuous normal distribution peaked at r_n with the dispersion σ equal to r_n , denoted by $P_{\text{norm}}(r_n, r_n)$. These parameter values allow us to cover all the scission neck configurations previously considered in Fig. 9.

If the drawn value of $r_{\text{neck}}^{\text{stop}}$ happens to be negative, its absolute value is taken. The resulting distributions seen in Fig. 10 with comparison to the previously used ones of Fig. 9(b) seem to be hardly distinguishable.

E. Final conditions and excitation energy

As can be seen, the introduction of a more involved Gaussian distribution on $r_{\text{neck}}^{\text{stop}}$ thresholds does not qualitatively change the final fragment mass distributions for thermal neutron-induced fission of ^{235}U . One can, in turn, apply a similar procedure to analyze the shapes of distributions for the systems of higher excitation energies. It is clear that the system, especially in the neck region, is less stable at

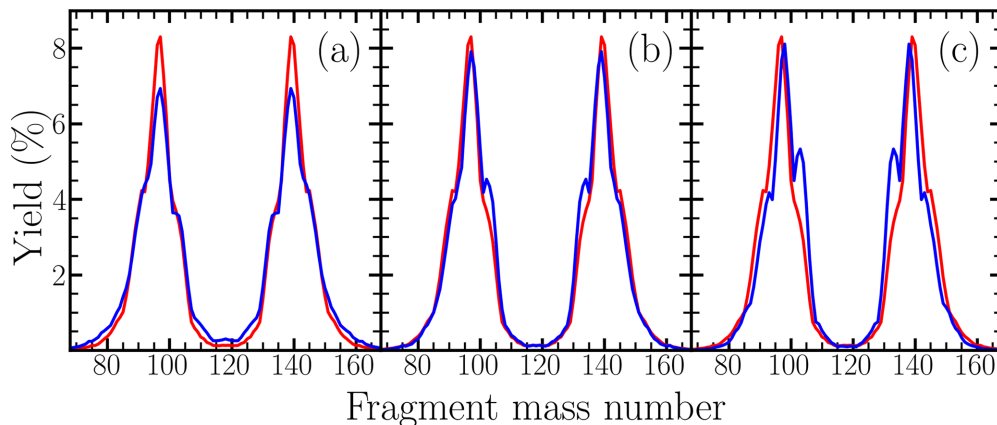


FIG. 9. Primary FMDs for thermal neutron-induced fission of ^{235}U calculated within random pick of $r_{\text{neck}}^{\text{stop}}$ (blue) defined on the following intervals: (a) $[0, 3r_n]$, (b) $[0, 2r_n]$, and (c) $[0, r_n]$, compared with analogous FMDs of Figs. 8(a)–8(c).

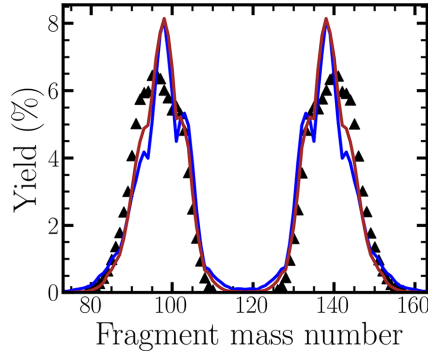


FIG. 10. Comparison of primary FMDs for thermal neutron-induced fission of ^{235}U calculated within Gaussian $P_{\text{norm}}(\mu = r_n, \sigma = r_n)$ (gray) and random picking (blue) distributions imposed on $r_{\text{neck}}^{\text{stop}}$.

higher temperatures. Some local surface vibration provoked by thermal nucleon motion can lead to a more rapid neck rupture, even when it is much greater than a nucleon's effective diameter. We then study the fast-neutron fission reaction, where $E_n = 14.8$ MeV. This means the excitation energy E^* exceeds the fission barrier V_B by almost 15 MeV. Here it is worth mentioning that at such initial excitation energies the compound nucleus may emit prescission neutrons during the fission process. Sometimes this kind of fission is called “multichance,” which undoubtedly affects the fission characteristics as shown, for example, in Ref. [14]. However, within the framework of this work we neglect this effect. The influence of the light particle emission both from the compound nucleus and from the fission fragments will be studied and accounted for in the future publications. The calculation is performed for the two variants of $r_{\text{neck}}^{\text{stop}}$ conditions, where first, $r_{\text{neck}}^{\text{stop}} = 2r_n$ (see further), and second, $r_{\text{neck}}^{\text{stop}}$ is randomly drawn with the probability given by the Gaussian distribution $P_{\text{norm}}(r_n, r_n)$. The results are shown in Fig. 11. It is seen that both theoretical estimates of FMDs exhibit a serious discrepancy compared with the experimental data in the region of symmetric fission channels.

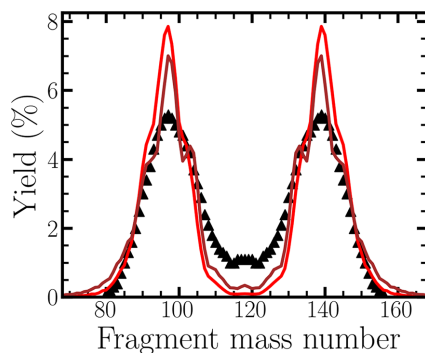


FIG. 11. Comparison of primary FMD with experimental data [47] for 15 MeV neutron-induced fission of ^{235}U (black triangles) with the ones calculated with Gaussian $P_{\text{norm}}(r_n, r_n)$ distribution (gray) and constant value $2r_n$ (red) of $r_{\text{neck}}^{\text{stop}}$.

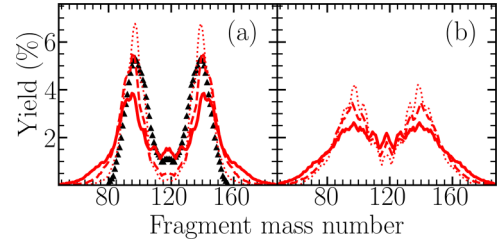


FIG. 12. Comparison of the primary FMDs for 15 MeV neutron-induced fission ^{235}U (left) and ^{236}U with 55 MeV excitation above the barrier top (right), calculated for the value of $r_{\text{neck}}^{\text{stop}}$ varying from $2r_n$ (dotted line), $3r_n$ (dashed line), and $4r_n$ (solid line). Experimental data [47] are also presented to make the comparison clearer.

This example illustrates, slightly in contrast to the thermal neutron-induced fission depicted in Fig. 10, an increased FMD sensitivity to the conditions defining the end of a Langevin trajectory. A good illustration of that statement is shown in Fig. 12, where the neck radius $r_{\text{neck}}^{\text{stop}}$ varies from $2r_n$ to $4r_n$ for the previously considered system with an excitation energy of about 15 MeV above the barrier (left panel). For comparison, we consider the uranium system with excitation energies already of 55 MeV in Fig. 12(b). With the condition for neck radius $r_{\text{neck}}^{\text{stop}} = r_n$, the form of the FMD is practically the same as for $2r_n$ while at higher values, e.g., $r_{\text{neck}}^{\text{stop}} > 4r_n$, it is difficult to say about the occurrence of the true neck. One can see that the symmetric yields of the final FMDs become closer to the measured values when the neck radius is higher than in the case of the thermal neutron-induced fission shown in Fig. 10 and varies between $2r_n$ and $3r_n$. A highly excited system of ^{236}U shows a similar tendency to enhance the symmetric fission channel.

F. Symmetric fission effect of very elongated systems

Now, let us return to the influence of the upper limit value of elongation, q_2^{max} , on the resulting FMDs—a problem already introduced in Sec. III B. In Fig. 13, the change of the FMD for a medium excited fissioning ^{235}U system as a function of q_2^{max} is presented. If q_2^{max} is continuously prolonged

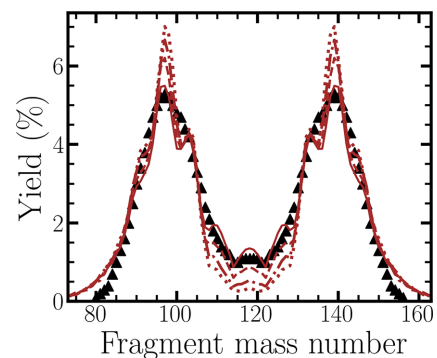


FIG. 13. Comparison of primary FMDs for 15 MeV neutron-induced fission of ^{235}U calculated within Gaussian $P_{\text{norm}}(r_n, r_n)$ distribution of $r_{\text{neck}}^{\text{stop}}$ with the upper limit of q_2^{max} as 2.35 (dotted line), 2.5 (dot-dashed line), 2.7 (dashed line), and 2.9 (solid line).

beyond the safe limit of 2.35, some growing numerical uncertainties in determining the PES and the transport coefficients may appear. Therefore, the temporal evolution of this nucleus is performed until this limit is achieved. We realize that ignoring such inaccuracies can obtain distributions that fit better the experimental data, but this accordance might as well be only accidental. Nonetheless, using the two-center Nilsson-like mean-field model and larger upper limit of elongation $q_2^{\max} = 2.9$ than we use allowed the authors to nicely describe the mass and total kinetic energy distributions for the thermal neutron-induced fission of ^{235}U and ^{239}Pu at an energy of 14.8 MeV with a realistic condition for $r_{\text{neck}}^{\text{stop}} = r_n$. As we already mentioned, the FMD obtained with $q_2^{\max} = 2.8\text{--}2.9$ is very close to its empirical results, as shown in Fig. 13. Its symmetric part grows gradually with increasing q_2^{\max} , reaching the experimentally measured value at $q_2^{\max} \approx 2.9$. In addition, the height of the asymmetric peak is then perfectly reproduced. Unfortunately, the yields for extremely asymmetric mass divisions are slightly overestimated in our approach.

Using the point-charge Coulomb interaction $E_{\text{Coul}} = e^2 \frac{Z_H Z_L}{R_{12}}$ (where H and L denote heavy and light fission fragment, respectively), supplemented by the kinetic energy of the relative motion of both fragments defined by Eqs. (22), we evaluate the average kinetic energy distributions $\overline{\text{TKE}}$ as a function of the heavy fragment mass, A_H , and present them in Fig. 14 for ^{235}U nucleus. The limit values of q_2^{\max} fixed respectively at 2.35 (blue curve) and 2.9 (orange curve) are distinguished for both reactions. At the higher value of the q_2^{\max} limit, especially for reactions with 14.8 MeV neutrons, the resulting distributions are noticeably closer to the experimental curves and fit well the error-bar areas.

Studying the results of Fig. 13, we notice that by the systematic extending of q_2^{\max} up to 2.9, we obtain a more substantial population of the highly elongated near-symmetric yields that contribute on average to the reduction of the TKE, mainly in part corresponding to symmetric fragmentation. However, this confirms the assumption made in Ref. [19], where from the analysis of TKEs and the quadrupole moments at the neck rupture of ^{236}U and ^{240}Pu it was found that at higher excitation energies there are special configurations of nuclei that have unusual elongated form.

Summarizing, the above-presented benchmark results obtained for selected uranium isotopes permitted us to fix the starting as well as the trajectory-termination conditions on the neck width, which are proved to be essential to reasonably reproduce empirical FMD and TKE distributions, especially at higher excitation energies. The other types of constraints are of ancillary nature, allowing for the elimination of trajectories that generally are not physical, thus reducing the calculation time. Moreover, a nontrivial relation between the final conditions and the excitation energy was observed, which still needs to be mathematically formulated.

IV. RESULTS AND DISCUSSION

After establishing the initial and termination (final) criteria for Langevin trajectories by studying the fission of the ^{235}U isotope as the exemplary case, let us broaden the applicability of the model in question to the other actinide nuclei.

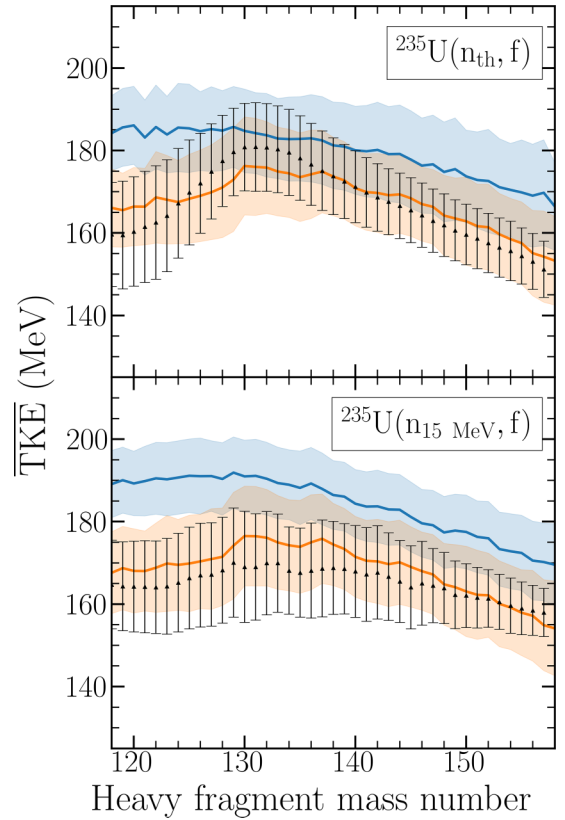


FIG. 14. Comparison of average total kinetic energy (TKE) distributions of primary fission fragments for 15 MeV neutron-induced fission of ^{235}U calculated within Gaussian distribution $P_{\text{norm}}(r_n, r_n)$ of $r_{\text{neck}}^{\text{stop}}$ with the upper limit q_2^{\max} equal to 2.35 (blue) and 2.9 (orange).

In particular, we will focus on the isotopes of ^{233}U , ^{239}Pu , ^{245}Cm , ^{249}Cf , and ^{255}Fm , for which experimental data on FMD are available. The resulting distributions for selected nuclei among these isotopic chains are illustrated in Fig. 15. The evaluated yields agree with experimental data in medium-heavy actinides, such as uranium, plutonium, and curium. Nevertheless, some larger discrepancies between estimated and empirical distributions are present in some heavy actinides of californium and fermium isotopes. Although the available experimental data refer to the distributions of secondary fragments (after the emission of light particles from compound nuclei as well as from fission fragments), the mutual shift of both those distributions by a couple of mass units for ^{250}Cf or the appearance of the symmetric-fission peak in our FMDs of ^{255}Fm cannot be fully explained by the effects of light particle evaporation alone. Also, as commonly known, in Cf and Fm nuclei, a rapid transition from the dominant asymmetric to symmetric fission mode, caused by adding two neutrons, is noticed. The reproduction of that is a particular challenge for our model. Recall that spontaneous or induced fission processes are probabilistic phenomena associated with overcoming the fission barrier between the ground state or some excited state and an exit point of the same energy located outside the barrier. In a quantum approach, the probability of passing the barrier is crudely dependent on the barrier

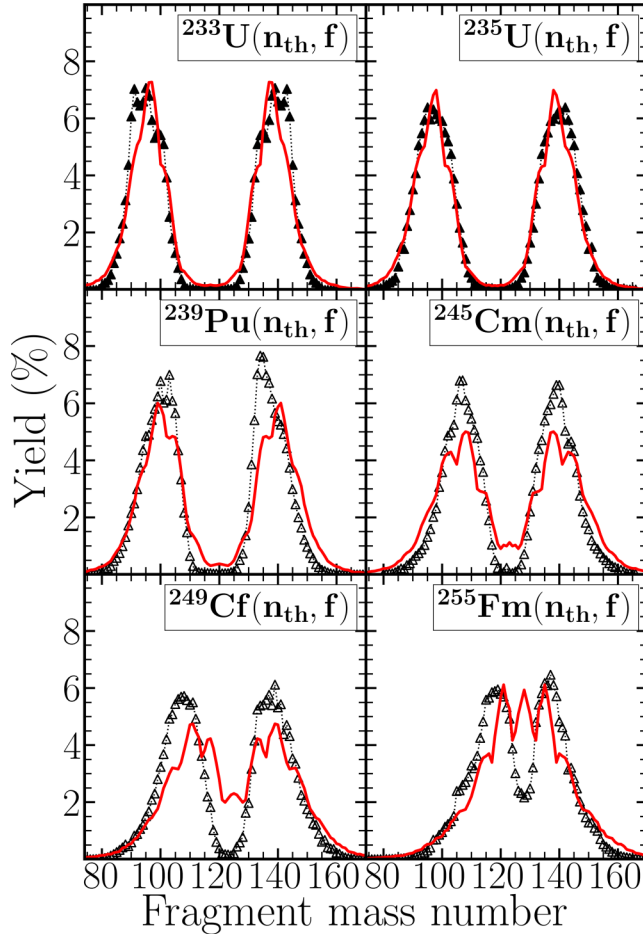


FIG. 15. Comparison of primary FMDs calculated in our Langevin approach within $P_{\text{norm}}(r_n, r_n)$ (solid red line) with primary (solid triangles) and secondary fission (open triangles) FMDs [45,48,49] for thermal neutron-induced fission of ^{233}U , ^{235}U , ^{239}Pu , ^{245}Cm , ^{249}Cf , and ^{255}Fm nuclei.

shape and the number of hits on the barrier per time unit. In contrast, in our Langevin semiclassical approach, the barrier is not “tunneled,” but it must be over-jumped by a system with kinetic energy greater than the barrier height in the initial evolution stage.

Using the method of determining the starting points given by formula (21), which are located slightly outside the outer saddle point, we perform the calculations of Langevin trajectories corresponding to the spontaneous fission for the following even-even nuclei series: ^{238}U , $^{238-244}\text{Pu}$, $^{244-248}\text{Cm}$, $^{252-256}\text{Cf}$, and $^{254-260}\text{Fm}$. The trajectory evolution is initiated using similar rules as in the case of induced fission, described in the previous sections. A particular value of $r_{\text{neck}}^{\text{stop}}$ for which a given trajectory is terminated at the pre-scission point is randomly drawn at the beginning of each trajectory with the Gaussian-distributed probability, $P_{\text{norm}}(r_n, r_n)$, as already used in the study of the ^{235}U isotope. Figure 16 illustrates the final FMDs for the spontaneous fission of the mentioned nuclei. At the background of generally satisfactory agreement between theory and experiment, mainly primary FMDs in these nuclei, we notice in ^{252}Cf that although the evaluated distributions

reproduce the dominance of asymmetric yields, they considerably overestimate the number of symmetrical fragments and are much too narrow. Note also that in $^{254,256}\text{Fm}$ and ^{256}Cf , the measured distributions include the effect of light-particle emission. However, both distributions compared in this figure differ dramatically.

Searching the discrete grids of the potential energy of californium and fermium nuclei with neutron numbers corresponding to the transition area from asymmetric to symmetric FMD, we find more than one point describing possible configurations of the exit from under the barrier. We, therefore, postulate that each such state should be treated as the starting point to perform the Langevin fission simulation. The final FMD thus obtained, say, “partial fragment mass distributions,” should be superimposed with appropriate weights to obtain the final FMD. A classical measure of these weights may be the values of the action integrals evaluated between given starting and exit points. The latter can be found either in the symmetric or asymmetric fission valley. This approach can be used mainly for Cf and Fm nuclei, in which the system decides where to go within a small bifurcation area in the PES after the fission barrier. Nevertheless, this issue is beyond the scope of this work and will be addressed in future investigations.

For a complete comparison, we also present the experimental distributions of primary and secondary fission fragments and the FMDs evaluated using the $P_{\text{norm}}(r_n, r_n)$ neck radius normal distribution. In addition, the above results will be contrasted with those calculated within the framework of the static BOA. This latter approach is based on an approximate solution of the eigenvalue problem of the three-dimensional collective Hamiltonian along the fission path. A more detailed description and relevant results for a wide range of even-even actinides can be found in Refs. [28,53]. Despite the different theoretical underpinnings of these two models, they both use identical PES and inertia parameters associated with our three-dimensional Fourier deformation space.

V. SUMMARY

In this work, we have systematically reported the dependence of the mass and total kinetic energy distributions of fission fragments in the low and medium excitation energy regimes, generally on the boundary conditions of the stochastic model used. For this purpose, quasiclassical Langevin equations are solved to simulate the stochastic nature of the fission dynamics of deformed excited compound actinide nuclei. To define this system of coupled equations with the constraint for the total energy conservation, the macroscopic-microscopic free (Helmholtz) energy, depending on the surface deformation and temperature, and the so-called transport coefficients must be precalculated. The numerical solutions using a discretization method are generated in the space of three Fourier surface deformations relevant for the fission process to describe the nucleus elongation, mass asymmetry, and neck thickness. As widely known, the impact of the nonaxiality degree of freedom on the PES is practically negligible outside the inner saddle and even much less in the vicinity of the scission configurations; thus it is totally neglected in this study. A simple way of defining the initial

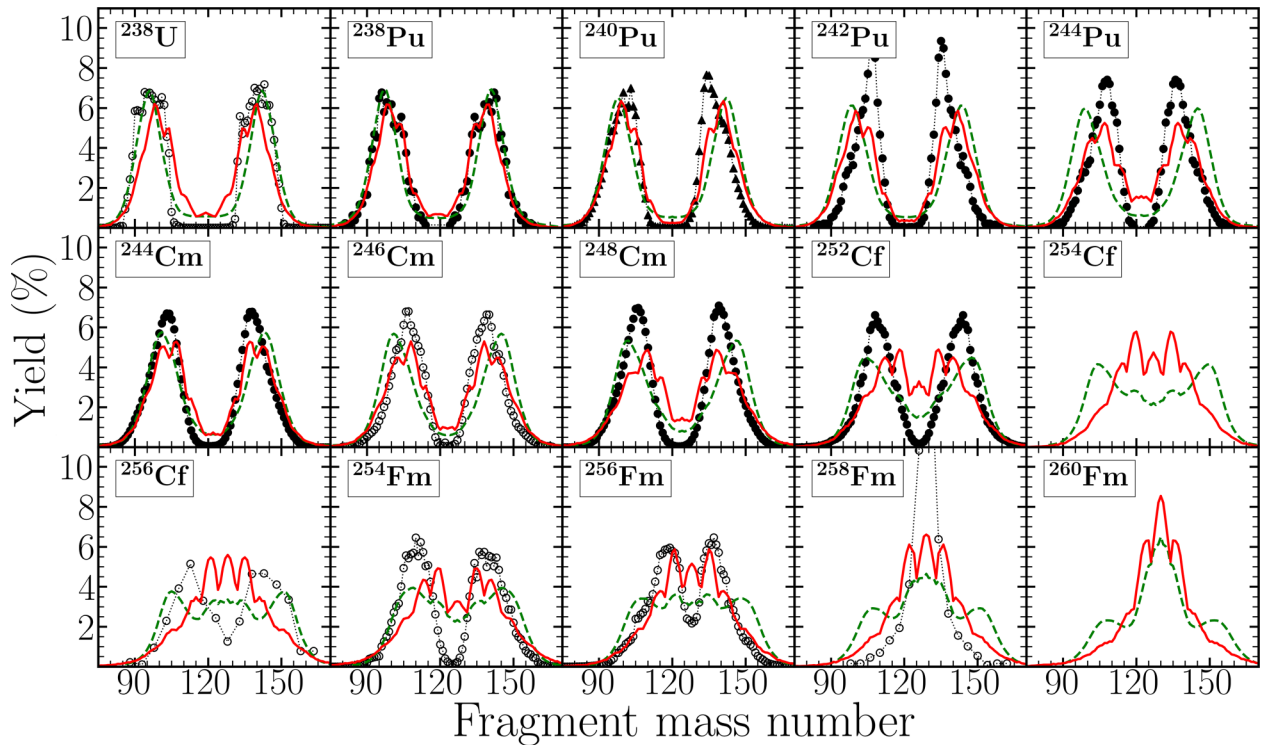


FIG. 16. Comparison of primary FMDs (solid red line) calculated in the Langevin approach within $P_{\text{norm}}(r_n, r_n)$ with experimental [48–52] primary (solid circles) and secondary (open circles) FMDs for spontaneous fission of U, Pu, Cm, Cf, and Fm nuclei also calculated with FMDs calculated within Born-Oppenheimer approximation (BOA) method [28] (green dashed lines).

and termination conditions for a single stochastic trajectory allows for generating hundreds of thousands of such trajectories in a reasonable time. Ultimately, the deformation properties of the final shape configurations of a large number of these trajectories are translated into statistical distributions of mass and kinetic energy.

We emphasize the importance of initial and trajectory-termination conditions, which can be considered independent of the particular realization of the Langevin framework. The latter condition seems particularly important, as it defines the “critical” width of the neck at which splitting the compound nucleus into fragments is highly probable. Since our calculations are carried out on a finite lattice of the potential energy function, we pay particular attention to accurately delineating its boundaries so that we can capture all essential fission modes, predominantly asymmetric, and, on the other hand, we do not consider nonphysical energy configurations which may show up in U isotopes at considerably large elongations.

After analyzing the conditions that are most important for our simulations and that determine the end of a single trajectory, we conclude that noticeably better results can be obtained if a normal probability distribution $P_{\text{norm}}(r_n, r_n)$ of the neck radii $r_{\text{neck}}^{\text{stop}}$ is used, instead of its fixed value. The peak of this distribution is, as expected, approximately located at the average value of the nucleon radius r_n while its standard deviation σ is also equal to r_n . As shown, with the increasing temperature, the $r_{\text{neck}}^{\text{stop}}$ radius must be shifted towards larger values.

Despite the relatively simplistic nature of the conditions discussed above, especially those describing the end of stochastic trajectories, the results for spontaneous and induced fission of even-even U, Pu, Cm, Cf, and Fm nuclei generally show satisfactory agreement with experimental data for medium and selected heavy actinides. However, we observe serious discrepancies in the overall behavior of the FMDs in the Cf and Fm series. Applying the aforementioned concept of superposition of several partial FMDs initiated from a different available exit from the barrier points would allow us to reproduce better the effect of the abrupt transition between asymmetric and symmetric fission modes. Further work is needed to improve the model’s ability to describe other fission characteristics, such as secondary FMDs and TKEs, corrected by the light particle evaporation effect.

ACKNOWLEDGMENTS

The authors are grateful to K. Pomorski and C. Schmitt for their support and fruitful discussions. This work is also partly supported by the Polish National Science Center by the SHENG-1 project (Grant No. 2018/30/Q/ST2/00185) and NAWA STER project “UMCS Doctoral Schools—Your Success in Globalized World of Science” (Grant No. BPI/STE/2021/1/00006/U/00001).

- [1] W. D. Myers and W. J. Swiatecki, *Nucl. Phys.* **81**, 1 (1966).
- [2] V. Strutinsky, *Nucl. Phys. A* **95**, 420 (1967).
- [3] V. Strutinsky, *Nucl. Phys. A* **122**, 1 (1968).
- [4] M. Brack *et al.*, *Rev. Mod. Phys.* **44**, 320 (1972).
- [5] P. Möller and J. Nix, *At. Data Nucl. Data Tables* **39**, 213 (1988).
- [6] P. Möller *et al.*, *At. Data Nucl. Data Tables* **109-110**, 1 (2016).
- [7] P. Jachimowicz, M. Kowal, and J. Skalski, *Phys. Rev. C* **95**, 014303 (2017).
- [8] M. Bender *et al.*, *J. Phys. G* **47**, 113002 (2020).
- [9] A. J. Sierk, *Phys. Rev. C* **96**, 034603 (2017).
- [10] K. Mazurek *et al.*, *Eur. Phys. J. A* **53**, 79 (2017).
- [11] M. D. Usang, F. A. Ivanyuk, C. Ishizuka, and S. Chiba, *Phys. Rev. C* **96**, 064617 (2017).
- [12] C. Ishizuka, M. D. Usang, F. A. Ivanyuk, J. A. Maruhn, K. Nishio, and S. Chiba, *Phys. Rev. C* **96**, 064616 (2017).
- [13] M. D. Usang *et al.*, *Sci. Rep.* **9**, 1525 (2019).
- [14] S. Tanaka, Y. Aritomo, Y. Miyamoto, K. Hirose, and K. Nishio, *Phys. Rev. C* **100**, 064605 (2019).
- [15] L.-L. Liu, X.-Z. Wu, Y.-J. Chen, C.-W. Shen, Z.-X. Li, and Z.-G. Ge, *Phys. Rev. C* **99**, 044614 (2019).
- [16] C. Ishizuka, X. Zhang, M. D. Usang, F. A. Ivanyuk, and S. Chiba, *Phys. Rev. C* **101**, 011601(R) (2020).
- [17] P. V. Kostryukov *et al.*, *Chin. Phys. C* **45**, 124108 (2021).
- [18] L.-L. Liu, Y.-J. Chen, X.-Z. Wu, Z.-X. Li, Z.-G. Ge, and K. Pomorski, *Phys. Rev. C* **103**, 044601 (2021).
- [19] K. Shimada, C. Ishizuka, F. A. Ivanyuk, and S. Chiba, *Phys. Rev. C* **104**, 054609 (2021).
- [20] L.-L. Liu, X.-Z. Wu, Y.-J. Chen, C.-W. Shen, Z.-G. Ge, and Z.-X. Li, *Phys. Rev. C* **105**, 034614 (2022).
- [21] C. Schmitt, K. Pomorski, B. Nerlo-Pomorska, and J. Bartel, *Phys. Rev. C* **95**, 034612 (2017).
- [22] Y. Abe, C. Grégoire, and H. Delagrangé, *J. Phys. Col.* **47**, 329 (1986).
- [23] S. Trentalange, S. E. Koonin, and A. J. Sierk, *Phys. Rev. C* **22**, 1159 (1980).
- [24] V. Pashkevich, *Nucl. Phys. A* **169**, 275 (1971).
- [25] G. Adeev, P. Cherdantsev, and I. Gamalya, *Phys. Lett. B* **35**, 125 (1971).
- [26] K. Pomorski and J. Bartel, *Int. J. Mod. Phys. E* **15**, 417 (2006).
- [27] J. Maruhn and W. Greiner, *Z. Phys.* **251**, 431 (1972).
- [28] K. Pomorski *et al.*, *Chin. Phys. C* **45**, 054109 (2021).
- [29] K. Pomorski and J. Dudek, *Phys. Rev. C* **67**, 044316 (2003).
- [30] J. Bardeen, L. N. Cooper, and J. R. Schrieffer, *Phys. Rev.* **108**, 1175 (1957).
- [31] A. Dobrowolski, K. Pomorski, and J. Bartel, *Comput. Phys. Commun.* **199**, 118 (2016).
- [32] B. Nerlo-Pomorska, K. Pomorski, and J. Bartel, *Int. J. Mod. Phys. E* **21**, 1250050 (2012).
- [33] B. Nerlo-Pomorska, K. Pomorski, and J. Bartel, *Phys. Rev. C* **74**, 034327 (2006).
- [34] R. Kubo, *Rep. Prog. Phys.* **29**, 255 (1966).
- [35] K. T. R. Davies, A. J. Sierk, and J. R. Nix, *Phys. Rev. C* **13**, 2385 (1976).
- [36] J. Bartel *et al.*, *Comput. Phys. Commun.* **241**, 139 (2019).
- [37] A. V. Ignatyuk, G. Smirenkin, and A. Tishin, *Sov. J. Nucl. Phys.* **21**, 255 (1975).
- [38] A. Ignatyuk, K. K. Istekov, and G. Smirenkin, *Sov. J. Nucl. Phys.* **29**, 450 (1979).
- [39] F. A. Ivanyuk, C. Ishizuka, M. D. Usang, and S. Chiba, *Phys. Rev. C* **97**, 054331 (2018).
- [40] F. A. Ivanyuk and K. Pomorski, *Phys. Rev. C* **53**, 1861 (1996).
- [41] H. Hofmann and D. Kiderlen, *Int. J. Mod. Phys. E* **07**, 243 (1998).
- [42] K. Pomorski, *Comput. Phys. Commun.* **174**, 181 (2006).
- [43] Y. Abe *et al.*, *Phys. Rep.* **275**, 49 (1996).
- [44] G. D. Adeev *et al.*, *Phys. Part. Nucl.* **36**, 733 (2005).
- [45] G. Simon *et al.*, *Nucl. Instrum. Methods Phys. Res., Sect. A* **286**, 220 (1990).
- [46] H. J. Krappe and K. Pomorski, *Theory of Nuclear Fission*, Lecture Notes in Physics Vol. 838 (Springer, Berlin, 2012).
- [47] B. Dyachenko, P. P. Kuzminov, and M. Tarasko, *Sov. J. Nucl. Phys.* **8**, 165 (1969).
- [48] E. K. Hulet *et al.*, *Phys. Rev. Lett.* **56**, 313 (1986).
- [49] K. H. Schmidt *et al.*, *Nucl. Data Sheets* **131**, 107 (2016).
- [50] L. Demattè *et al.*, *Nucl. Phys. A* **617**, 331 (1997).
- [51] F. Pleasonton, R. L. Ferguson, F. Plasil, and C. E. Bemis, Jr., *Phys. Rev. C* **8**, 1018 (1973).
- [52] D. C. Hoffman, J. B. Wilhelmy, J. Weber, W. R. Daniels, E. K. Hulet, R. W. Loughheed, J. H. Landrum, J. F. Wild, and R. J. Dupzyk, *Phys. Rev. C* **21**, 972 (1980).
- [53] K. Pomorski, F. A. Ivanyuk, and B. Nerlo-Pomorska, *Eur. Phys. J. A* **53**, 59 (2017).